Singular optimal driving cycles of stochastic pumps

Ilana Bogod and Saar Rahav [*]

Schulich Faculty of Chemistry, Technion–Israel Institute of Technology, Haifa 3200008, Israel

The investigation of optimal processes has a long history in the field of thermodynamics. It is well-known that finite-time processes which minimize dissipation often exhibit discontinuities. We use a combination of numerical and analytical approaches to study the driving cycle that maximizes the output in a simple model of a stochastic pump: a system driven out of equilibrium by a cyclic variation of external parameters. We find that this optimal solution is singular, with an infinite rate of switching between sets of parameters. The appearance of such singular solutions in thermodynamic processes is surprising, but we argue that such solutions are expected to be quite common in models whose dynamics exhibit exponential relaxation, as long as the driving period is not externally fixed and is allowed to be arbitrarily short. Our results have implications to artificial molecular motors that are driven in a cyclic manner.

I. INTRODUCTION

Questions regarding the optimal way of performing a task or operating a machine fit naturally into the scope of the theory of thermodynamics [1]. Examples range from Carnot's celebrated work on heat engines [2] to more modern geometrical approaches [3–5]. Technological advances allow the manipulation and observation of molecular motors, nanoscale machines, and microscopic information or heat engines. The theory of stochastic thermodynamics offers a consistent and illuminating thermodynamic description of such small out-of-equilibrium systems [6–9]. In particular, the theory accounts for the unavoidable fluctuations due to the random interactions of a small system with its environment. This research effort has led to several fundamental results that enhance our understanding of out-of-equilibrium systems and processes, such as fluctuation relations [10–15], thermodynamic uncertainty relations [16–19], and a renewed interest in the thermodynamics of information [20]. The predictions of the theory were tested experimentally using colloidal particles [21–25], RNA hairpins [26,27], single-electron boxes [28,29], molecular motors [30,31], and more [32].

A substantial body of research was devoted to the investigation of the role of optimal processes in stochastic thermodynamics. Schmiedl and Seifert pointed out that finite-time processes which minimize the work often exhibit discontinuities at initial and final times [33]. The appearance of such discontinuities is known in control theory [34], but is somewhat surprising in the context of thermodynamic pro-

cesses. This result therefore generated considerable interest, and similar discontinuities were found in several other out-of-equilibrium systems [35–37]. Several works showed how to apply techniques from control theory to stochastic thermodynamics problems, see, e.g., Refs. [37–40]. While much of the work on the subject focused on finite-time transitions between two states, several papers studied the optimal operation of periodically driven systems [41–44].

In this paper, we investigate the optimal driving cycles of stochastic pumps. The term stochastic pump is used to describe models with discrete states which are driven away from equilibrium due to cyclic variation of system parameters. Several experimental realizations of artificial molecular machines can be modeled as stochastic pumps [45–48]. Various aspects of stochastic pumps were studied theoretically in the last two decades. These include (i) the underlying similarities and differences between steady states and periodically driven systems [49,50], (ii) adiabatic and geometrical pumping [51–54], and the no-pumping theorem [55–62], as well as other aspects of such pumps [63–71]. Additional results are summarized in several review papers devoted to this topic [72–75].

The optimization problem studied here exhibits two aspects that should be highlighted. One is the presence of a resisting external force. The pump performs work against this external force. Much of the existing literature on optimal stochastic thermodynamic processes was centered on minimizing dissipation when transitioning between two states or maximizing a pump current. By focusing on the pump's power output, we set up a different optimization problem. The second aspect is the full freedom of choosing the time dependence of parameters (within a predefined range). Specifically, there are no additional restrictions on the shape of the driving cycle or its period. This in turn means that there are no evident approximations that can be used to reduce the dimension of the optimization problem. Nevertheless, progress can be made by considering a simple two-site model of a stochastic pump. We use a combination of analytical and numerical techniques

[*]rahavs@technion.ac.il

to identify the driving cycles that maximize the power output. Interestingly, these optimal cycles turn out to be singular. Specifically, the external parameters alternate between two sets of values. The maximum output is found when the rate of switching between the sets approaches infinity. While such solutions are known in the literature on control theory [76,77], they are uncommon in the context of thermodynamic processes. Our results therefore add another facet to the study of the stochastic thermodynamics of optimal processes.

Our paper is structured as follows. In Sec. II, we discuss some qualitative aspects of artificial molecular machines that serve as motivation for the problem investigated in what follows. We present the model and define the relevant thermodynamic observables in Sec. III. Section IV describes some physically motivated restrictions that we place on the driving cycles. Such restrictions are needed to make the optimization problem well-defined. In Sec. V, we identify and study a family of driving cycles which are a good candidates for optimal solutions. We then demonstrate in Sec. VI that these cycles locally maximize the output of the pump. A numerical approach based on genetic algorithms is presented and applied in Sec. VII. It suggests that the optimal solution is attained when the period of the cycles from Sec. V approaches zero. In Sec. VIII, we study a regularized problem in which a small cost is associated to changes in site energies. A good agreement between the analytical and numerical approaches is found for this regularized problem. Furthermore, the regularized solutions approach the their singular counterparts from Sec. VII when the additional cost is decreased. Finally, we discuss the implications and generality of our results in Sec. IX.

II. MOTIVATION: PERIODICALLY DRIVEN MOLECULAR MACHINES

Our bodies are teeming with proteins that act as machines. Life would not have been possible without molecules that transport cargo, copy or translate nucleic acids, assist cell division, and more [78]. The fascination with molecules that can act as machines inspired chemists to design and synthesize artificial molecular machines. The success of this fascinating research effort has resulted in the awarding of the 2016 Nobel Prize in Chemistry, which was awarded to Sauvage, Stoddart, and Feringa.

The work presented below is motivated by a certain type of artificially made molecular machines, built from complexes of mechanically interlocked molecules [48]. As pioneered by the groups of Stoddart and Leigh, such mechanically interlocked molecules can be operated as machines by making a closed cycle of changes in the molecules or in their environment. The motion of such molecules in solution is highly overdamped and exhibits relatively large fluctuations. The dynamics is often described in terms of transitions between a few metastable conformations. Since the changes made during the cycle are often local, it is natural to model them theoretically as externally controlled changes in the free energy of the metastable states and barriers between them. When these are varied cyclically, the system is operated as a stochastic pump. Artificial molecular machines of this kind include switches, shuttles, and rotary motors. Specific examples and details regarding

the chemical structure and operation can be found in several review papers [45–48,74].

Figure 1(a) heuristically depicts a part of a molecular machine of this kind. A small ringlike molecule can move along the backbone of a larger molecule. a and b are energetically favorable binding sites for the ring due to hydrogen bonds or van der Waals interactions. The purple ball represents part of the backbone that acts as a barrier.

The free energy landscape of such a system is the multidimensional generalization of the simple free-energy landscape shown in Fig. 1(b). The motion in such a landscape consists of relatively rapid local equilibration in the wells, with occasional transitions between the wells. When $G^{\ddagger} - G_a \gg k_B T$, the transitions between the metastable configuration are thermally activated, with rates

$$R_{ba} \simeq \nu \exp\left[-\frac{G^{\ddagger} - G_a}{k_B T}\right]. \tag{1}$$

Here G_a and $G^{\ddagger}$ are the free energies of the configuration a and the ring at the top of the barrier, and ν is an attempt frequency. For overdamped dynamics, the expression Eq. (1) can be justified using Kramers rate theory [79]. Such rates are commonly used to model the dynamics of artificial molecular machines.

The existence of this class of periodically driven molecular machines raises various fundamental questions regarding their thermodynamics. What is the optimal way of driving such systems? Should externally controlled parameters be varied gradually or in an abrupt manner? Here we study how the output of such systems should be maximized. The number of time-dependent control parameters makes this a nontrivial problem. We therefore focus on a simple example. Consider the system depicted in Fig. 1(c). It has two metastable configurations (which we call sites) and two possible transition between them. We imagine that the free energies of the two sites and the barriers can be manipulated externally. Our model also includes a resisting force f that makes counterclockwise transitions more likely. (Strictly speaking, f is a shorthand for the force times the distance between sites, and thus has units of energy.) The system is operated as a pump when the ring is driven against this resisting force.

Our model is quite similar to a molecular machine realized by the Leigh group [80]. Their artificial molecular motor has the structure depicted in Fig. 1(c), but its kinetics differs from the one we explore in several important aspects. The system realized in Ref. [80] was autonomous, and furthermore exhibited nontrivial coupling between the position of the smaller ringlike molecule and the kinetics of the barriers. In contrast, we assume that the barriers are externally controlled in a way that does not depend on the sites. In addition, the machine of Ref. [80] had no resisting force. Nevertheless, this beautiful experiment demonstrates the feasibility of molecular machines of this kind and motivates the theoretical investigation of their dynamics and thermodynamics.

III. THE TWO-SITE MODEL

The system we examine is a two-site stochastic pump, as depicted in Fig. 1(c). Each site has an energy that can be manipulated externally. (To simplify the terminology, we will
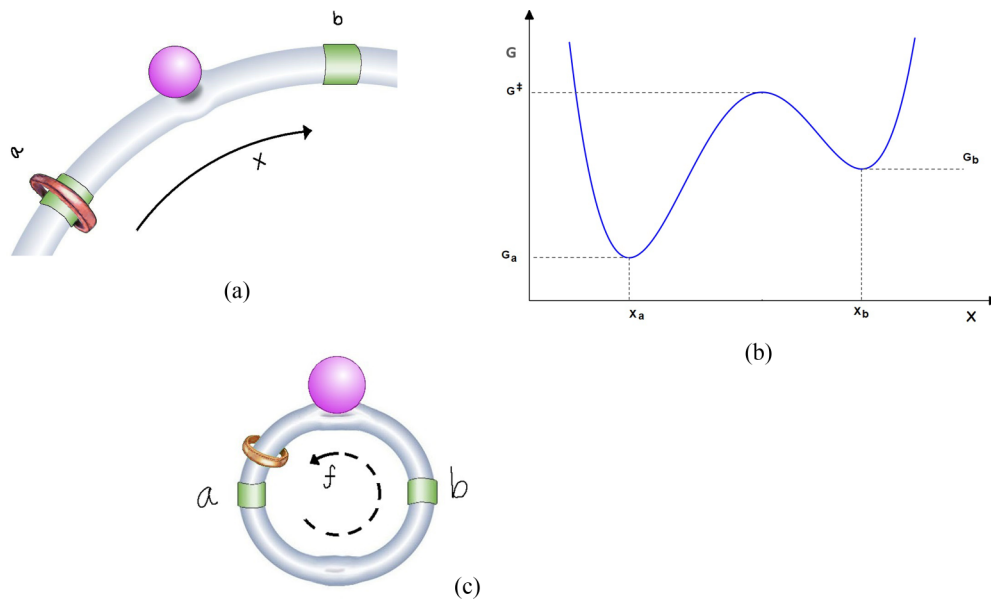
FIG. 1. Heuristic depiction of artificial molecular machines that are modeled as stochastic pumps. (a) Part of a mechanically interlocked system in which a small ringlike molecule can move along a larger backbone molecule. The two green regions depict areas capable of forming favorable noncovalent interactions between the ring and backbone. The dent and purple ball represent a region with steric or repulsive interactions that acts as a local barrier. (The barrier is lower when the ball is absent.) (b) A one-dimensional free energy landscape can be used to describe the system depicted in Fig. 1(a). The minima represent the landing sites and the maximum represents the barrier. The free energies of the wells and the barrier can be modified by replacing the side groups attached to the backbone. The system is typically in a solvent at room temperature. As a result, transitions between the wells are thermally activated, with rates given by Eq. (1). (c) A depiction of the model studied in this paper. A small ringlike molecule can move between two stable landing sites on a larger ring. Each of the transition paths has its own barrier.

refer to the site and barrier free energies as energies in the following. The two distinct bidirectional transitions have local energy barriers $B_{1,2}$ that must be overcome for a transition to occur. The resisting force f makes counter-clockwise transitions more likely by biasing the transitions. These rates are taken to be Markovian and thermally activated, meaning that the stochastic pump is assumed to be in contact with an external reservoir with a well-defined temperature T, for instance, a large quantity of solvent molecules in thermal equilibrium. We consider rates of the form

$$R_{ba}^{(1)} = \exp\left[\frac{E_a - B_1 - \theta f}{T}\right],$$

$$R_{ab}^{(1)} = \exp\left[\frac{E_b - B_1 + (1-\theta)f}{T}\right],$$

$$R_{ba}^{(2)} = \exp\left[\frac{E_a - B_2 + (1-\theta)f}{T}\right],$$

$$R_{ab}^{(2)} = \exp\left[\frac{E_b - B_2 - \theta f}{T}\right]. \tag{2}$$

Here $R_{ba}^{(1)}$ is the rate of transitions from site a to site b that are made via mechanism 1. Similar notation is used for the rest of the rates. $0 \leqslant \theta \leqslant 1$ is a load distribution factor that describes the way that the resisting force is divided between two opposite transitions.

Two comments regarding the rates in Eq. (2) are in order. These rates were brought to a simple form that would simplify the subsequent calculations. Specifically, we work in units where $k_B = 1$. We also measure energies and barriers with

respect to reference values E_0 and B_0. We then rescale time to absorb the factor of $\tilde{\nu} = \nu \exp[-\frac{B_0 - E_0}{T}]$ that is common to all rates. This crucially means that $E > B$ in Eq. (2) does not mean that the metastable state is destroyed. In fact, we assume that the sites are stable for all the values of the site energies and barriers used below, and that as a result the thermal activation description of the transitions remains valid.

The two-site system can be operated as a stochastic pump by varying the two energies $E_a(t)$, $E_b(t)$, and the two barriers $B_1(t)$, $B_2(t)$ periodically in time. In contrast, the temperature and the resisting force are kept fixed. In the following, we also assume that we are given a period τ, so the externally controlled parameters must satisfy $E_i(t + \tau) = E_i(t)$ and $B_j(t + \tau) = B_j(t)$. Note that demanding an external period of τ allows for time dependence that exhibits smaller periods, as long as an integer number of periods are completed within time τ.

The probability to find the system in the sites, $P_a(t)$ and $P_b(t) = 1 - P_a(t)$, evolves according to the time-dependent master equation

$$\frac{d\vec{P}}{dt} = \mathbf{R}(t)\vec{P}(t), \tag{3}$$

with $\vec{P} = \begin{pmatrix} P_a \\ P_b \end{pmatrix}$, and

$$\mathbf{R}(t) = \begin{pmatrix} -R_{ba}^{(1)} - R_{ba}^{(2)} & R_{ab}^{(1)} + R_{ab}^{(2)} \\ R_{ba}^{(1)} + R_{ba}^{(2)} & -R_{ab}^{(1)} - R_{ab}^{(2)} \end{pmatrix}. \tag{4}$$

When the transition rates are periodic in time, the master equation has a periodic asymptotic solution satisfying $\vec{P}^{(ps)}(t + \tau) = \vec{P}^{(ps)}(t)$. In the following, we will be interested in properties of the pump in this periodic solution, ignoring transient solutions. We will therefore omit the superscript (*ps*) in the rest of the paper, since we will never consider any other solutions of the master equation.

Changing the energies and barriers periodically does not ensure that the system is operated as a stochastic pump. Calling the system a pump implies that the external variation of parameters is the source of energy that drives the system and that this energy is transduced to some useful form of work. Here this means work done against the resisting force *f*. This is achieved by making more $a \to b$ than $b \to a$ transitions using mechanism 1, and similarly more $b \to a$ transitions using mechanism 2.

This qualitative description can be made precise by calculating the energy that the pump exchanges with the outside world. The work that is done on the pump in each cycle is given by

$$W = \int_t^{t+\tau} dt' [\dot{E}_a(t')P_a(t') + \dot{E}_b(t')P_b(t')]. \quad (5)$$

The useful output is due to transitions against the resisting force. This definition is motivated by the ability to interpret the transitions as involving the storage or release of useful energy, e.g., by lifting a mass or compressing a spring. The energy output during a cycle is given by

$$\Phi = f \int_t^{t+\tau} dt' \big[R_{ba}^{(1)}(t')P_a(t') - R_{ab}^{(1)}(t')P_b(t') + R_{ab}^{(2)}(t')P_b(t') \\ - R_{ba}^{(2)}(t')P_a(t') \big]. \quad (6)$$

The system is operated as a stochastic pumps when $W \geqslant \Phi > 0$. In this regime, the pump's efficiency is

$$\eta = \frac{\Phi}{W}. \quad (7)$$

IV. STATING THE OPTIMIZATION PROBLEM

Our goal is to find the periodic functions $E_a(t)$, $E_b(t)$, $B_1(t)$, and $B_2(t)$ that would result in maximal output Φ. For a fixed period, this is equivalent to maximizing the output power Φ/τ. Equation (6) allows us to express the output as a functional of the energies and barriers. Some consideration reveals that this optimization problem is not well posed. During times in the cycle when probability flows from *a* to *b*, it is beneficial to take $E_a(t) \to \infty$ and $E_b(t) \to -\infty$ and also $B_2(t) \to \infty$ and $B_1(t) \to -\infty$. Similar considerations apply when the probability flows from *b* to *a*.

This tendency of sending the parameters to infinity is unphysical and therefore unwanted. It is not realistic to expect that in any real-world realization of a stochastic pump, the experimentalists will have arbitrary freedom to control the system's parameters. We will therefore assume that the energies can be varied in a limited range:

$$0 \leqslant E_a(t), E_b(t) \leqslant E_{\max}. \quad (8)$$

Similarly, we will demand that both barriers satisfy

$$0 \leqslant B_1(t), B_2(t). \quad (9)$$

Note that we do allow the barriers to be arbitrarily large, since being able to completely prevent transitions at certain times can be beneficial, and is not that different from the solution that would be found when using a finite but very large barrier height. We note that the lower bound of barriers can be chosen to be 0, for convenience, since it is measured from an almost arbitrary reference point, as discussed earlier.

With these restrictions on the values of the energies and barriers, the problem of finding the driving protocol that would maximize the output Eq. (6) seems well posed. As will become clear in the following, even such a well-posed problem can exhibit singular optimal solutions.

V. A FAMILY OF CANDIDATES FOR THE OPTIMAL SOLUTION

The model depicted in Fig. 1(c) is simple enough for one to use physical intuition to identify driving protocols that are good candidates for optimal solutions. Consider a driving protocol with a period τ. In any nontrivial cycle, the probability must flow between sites *a* and *b*. As the overall phase of the cycle is arbitrary, we can assume that probability flows from *a* to *b* in the first half of the cycle and in the opposite direction in the second half. We can try to maximize the output in the first half of the cycle by preventing transitions through 2, since they would contribute negatively. Similarly, we gain more output by increasing the energy difference $E_a - E_b$. This results in $E_a(t) = E_{\max}$, $E_b(t) = 0$, $B_1(t) = 0$, and $B_2(t) = \infty$ for $0 \leqslant t < \frac{\tau}{2}$. In the other half of the cycle, probability flows from *b* to *a*. Repeating the same considerations suggests taking $E_a(t) = 0$, $E_b(t) = E_{\max}$, $B_1(t) = \infty$, and $B_2(t) = 0$ for $\frac{\tau}{2} \leqslant t < \tau$. Below we calculate the solution of the master equation with this driving protocol and study its properties, focusing on the output.

This driving cycle has piecewise constant rates, which can attain only two nonvanishing values. For $0 \leqslant t < \frac{\tau}{2}$, we have

$$R_{ba}^{(1)}(t) = \exp\left[\frac{E_{\max} - f\theta}{T}\right] \equiv K_1, \quad (10)$$

$$R_{ab}^{(1)}(t) = \exp\left[\frac{f(1-\theta)}{T}\right] \equiv K_2, \quad (11)$$

and $R_{ba}^{(2)}(t) = R_{ab}^{(2)}(t) = 0$. The transition rate matrix in this part of the cycle is given by

$$\mathbf{R}_1 = \begin{pmatrix} -K_1 & K_2 \\ K_1 & -K_2 \end{pmatrix}. \quad (12)$$

The propagator for the first half of the cycle can be calculated with the help of the spectral decomposition of $\mathbf{R}_1$; see Appendix A for details. We find

$$\mathbf{U}_1 = e^{\mathbf{R}_1 \frac{\tau}{2}} = \frac{1}{K_1 + K_2} \begin{pmatrix} K_2 + xK_1 & K_2(1-x) \\ K_1(1-x) & K_1 + xK_2 \end{pmatrix}, \quad (13)$$

where $x \equiv \exp[-(K_1 + K_2)\frac{\tau}{2}]$ is a useful abbreviation.

The second half of the cycle is treated in the same way. Here

$$\mathbf{R}_2 = \begin{pmatrix} -K_2 & K_1 \\ K_2 & -K_1 \end{pmatrix} \qquad (14)$$

and

$$\mathbf{U}_2 = e^{\mathbf{R}_2 \frac{\tau}{2}} = \frac{1}{K_1 + K_2} \begin{pmatrix} K_1 + xK_2 & K_1(1-x) \\ K_2(1-x) & K_2 + xK_1 \end{pmatrix}. \qquad (15)$$

The periodic solution of the master equation satisfies

$$\vec{P}(\tau) = \mathbf{U}_2 \mathbf{U}_1 \vec{P}(0). \qquad (16)$$

The two-site model exhibits some symmetry. In particular, states a and b play equivalent roles at different times during the cycle. Here, this means that the dynamics during the second half of the cycle is identical to that of the first half as long as one replaces $a \leftrightarrow b$ and $1 \leftrightarrow 2$. One can therefore replace Eq. (16) with

$$\begin{pmatrix} P_b(0) \\ P_a(0) \end{pmatrix} = \begin{pmatrix} P_a(\tau/2) \\ P_b(\tau/2) \end{pmatrix} = \mathbf{U}_1 \begin{pmatrix} P_a(0) \\ P_b(0) \end{pmatrix}. \qquad (17)$$

After a straightforward calculation, one finds

$$P_a(0) = \frac{K_1 + xK_2}{(K_1 + K_2)(1 + x)} \qquad (18)$$

and

$$P_b(0) = 1 - P_a(0) = \frac{K_2 + xK_1}{(K_1 + K_2)(1 + x)}. \qquad (19)$$

The probability after half a cycle can be found with the help of Eq. (17), e.g., $P_a(\tau/2) = P_b(0)$.

Calculation of the power output of the pump is simplified considerably for this cycle because at any given time only transitions that use one of the mechanisms are possible. This creates a strong coupling between the currents and the changes of probabilities during the cycle. The contribution of transitions through link 1 to the output comes from the first half of the cycle and is equal to $f(P_a(0) - P_a(\tau/2))$. Taking into account also a similar contribution from the second half of the cycle, we have

$$\Phi = f(P_a(0) - P_a(\tau/2)) + f(P_b(\tau/2) - P_b(\tau)). \qquad (20)$$

Substituting the value of the probabilities at different times results in

$$\Phi = \frac{2f(K_1 - K_2)(1 - x)}{(K_1 + K_2)(1 + x)}. \qquad (21)$$

Note that this output is indeed positive as long as $K_1 > K_2$ or, equivalently, $E_{\max} > f$.

The work that is done on the pump originates from the changes in the energies at times $t = 0, \frac{\tau}{2}$. It is given by

$$W = E_{\max} \left[P_a(0) - P_b(0) - P_a\left(\frac{\tau}{2}\right) + P_b\left(\frac{\tau}{2}\right) \right]. \qquad (22)$$

Substituting the probabilities leads to

$$W = \frac{2E_{\max}(K_1 - K_2)(1 - x)}{(K_1 + K_2)(1 + x)}. \qquad (23)$$

The efficiency of the pump in this driving cycle turns out to be particularly simple:

$$\eta = \frac{f}{E_{\max}}. \qquad (24)$$

An equivalent expression for the efficiency was previously found in a similar three-site model of a stochastic pump [65].

We point out that the τ periodicity of energies allows for solutions that are composed of a combination of cycles with smaller periods. Of particular interest are ones composed of n repetitions of a cycle with a period $\tau' = \tau/n$. The solution given above is easily modified to apply for the these cycles, meaning that the calculations above actually describe a family of solutions with different periods.

VI. LOCAL OPTIMALITY OF THE DRIVING PROTOCOLS

In this section, we examine the stability of the solutions studied in Sec. V to small perturbations. Specifically, we examine small changes in the switching time and in the energies and barriers but not in the overall period τ. We find below that such changes reduce the output of the cycles, meaning that these cycles locally maximize the output.

A. Stability to small changes in the switching time

Let us consider a cycle that is deformed by slightly modifying the duration of the two half cycles, so the overall period of the cycle is kept fixed. Without losing generality, we can assume that the time in which the rate matrix is changes from $\mathbf{R}_1$ to $\mathbf{R}_2$ is now $\tau/2 + \delta t$ instead of $\tau/2$. We wish to find out how such a change will affect the output of the cycle. For small δt, this can be studied using perturbation theory. The calculation is almost straightforward, but care should be taken because the perturbation also results in small corrections to the periodic solution of the master equation in Eq. (3), and they must be taken into account.

The propagator of the first segment of the cycle is now given by

$$\mathbf{U}_1' = e^{\mathbf{R}_1(\frac{\tau}{2} + \delta t)} = \mathbf{U}_1 + \delta t x \mathbf{R}_1 - \frac{\delta t^2 x}{2}(K_1 + K_2)\mathbf{R}_1 + O(\delta t^3). \qquad (25)$$

Here we kept terms up to order δt^2, since it will become clear that this is the leading order correction to the output of the cycle. Similarly, the propagator of the second segment of the cycle is

$$\mathbf{U}_2' = e^{\mathbf{R}_2(\frac{\tau}{2} - \delta t)} = \mathbf{U}_2 - \delta t x \mathbf{R}_2 - \frac{\delta t^2 x}{2}(K_1 + K_2)\mathbf{R}_2 + O(\delta t^3). \qquad (26)$$

The propagator of the full cycle is simply the product $\mathbf{U}_2' \mathbf{U}_1'$. To second order, we find

$$\mathbf{U}' = \mathbf{U}_2 \mathbf{U}_1 + \delta t x (K_1 - K_2) \begin{pmatrix} -1 & -1 \\ 1 & 1 \end{pmatrix}$$

$$+ \frac{\delta t^2}{2} x (K_1^2 - K_2^2) \begin{pmatrix} -1 & -1 \\ 1 & 1 \end{pmatrix} + O(\delta t^3). \qquad (27)$$

The appearance of the matrix $\begin{pmatrix} -1 & -1 \\ 1 & 1 \end{pmatrix}$ is a result of conservation of probability and the fact that the system has only two sites. As a result, deviations from the unperturbed periodic solutions are always proportional to $\begin{pmatrix} 1 \\ -1 \end{pmatrix}$ to avoid violating the demand that $P'_A(t) + P'_B(t) = 1$. Multiplication of the matrix above and any normalized probability distribution results in a term which is proportional to the vector $\begin{pmatrix} 1 \\ -1 \end{pmatrix}$.

The periodic solution of the perturbed cycle can be found with the help of Eq. (16), where one uses the modified propagator in Eq. (27). Some algebra results in

$$P'_A(0) = \frac{K_1 + xK_2}{(K_1 + K_2)(1 + x)} - \delta t \frac{x}{1 - x^2}(K_1 - K_2)$$
$$- \frac{\delta t^2}{2} \frac{x}{1 - x^2}\left(K_1^2 - K_2^2\right) + O(\delta t^3), \qquad (28)$$

where, as always, $P'_B(0) = 1 - P'_A(0)$. The calculation of the output requires knowledge of the probabilities at the switching time $t = \tau/2 + \delta t$. These can be calculated from the probabilities at $t = 0$ with the help of the propagator $\mathbf{U}'_1$. A short calculation results in

$$P'_A\left(\frac{\tau}{2} + \delta t\right) = \frac{K_2 + xK_1}{(K_1 + K_2)(1 + x)} - \delta t \frac{x}{1 - x^2}(K_1 - K_2)$$
$$+ \frac{\delta t^2}{2} \frac{x}{1 - x^2}\left(K_1^2 - K_2^2\right) + O(\delta t^3). \qquad (29)$$

The calculation of the output is essentially the same as for the unperturbed cycle. During the first segment of the cycle, a probability of $P'_A(0) - P'_A(\frac{\tau}{2} + \delta t)$ flows from site a to site b. In the second segment of the cycle, the same probability flows back. In both segments, one of the pathways is open and the other is closed, so this flow must contribute positively to the output. As a result, the output is given by

$$\Phi' = 2f\left[P'_A(0) - P'_A\left(\frac{\tau}{2} + \delta t\right)\right] = \frac{2f(K_1 - K_2)(1 - x)}{(K_1 + K_2)(1 + x)}$$
$$- \delta t^2 \frac{2fx}{1 - x^2}\left(K_1^2 - K_2^2\right) + O(\delta t^3). \qquad (30)$$

The first term on the right-hand side of Eq. (30) is the output of the unperturbed cycle. We note that $0 < x < 1$ and $K_1 > K_2$. It is therefore clear that small changes in the switching time always reduce the output of a cycle, as long as the overall period is unchanged. The argument also covers changes in the time of the switch from $\mathbf{R}_2$ to $\mathbf{R}_1$. This can be seen by changing the origin of time to the time when $\mathbf{R}_2$ is replaced by $\mathbf{R}_1$, which maps the problem to the one studied above.

B. Linear response corrections due to small changes in the barriers and energies

We now consider how the power output of the solutions discussed in Sec. V is affected if the time dependence of the energies and barriers is slightly modified. To this end, we write

$$\mathbf{R}'(t) = \mathbf{R}(t) + \delta\mathbf{R}(t), \qquad (31)$$

where both $\mathbf{R}(t)$ and $\delta\mathbf{R}(t)$ are periodic with the same period τ. In the following, we consider $\delta\mathbf{R}(t)$ to be small. We then examine the linear order corrections to the power output from such perturbations. The small changes in the rates result in a perturbed periodic state:

$$\vec{P}'(t) = \vec{P}(t) + \delta\vec{P}(t). \qquad (32)$$

Here $\vec{P}$ is the solution of the unperturbed problem:

$$\frac{d\vec{P}}{dt} = \mathbf{R}(t)\vec{P}(t). \qquad (33)$$

This unperturbed solution can be calculated explicitly using the spectral decomposition found in Appendix A and the initial condition Eq. (18). A straightforward calculation results in

$$\vec{P}(\tilde{t}) = \frac{1}{(K_1 + K_2)(1 + x)} \begin{cases} \begin{pmatrix} K_2(1 + x) + x_{\tilde{t}}(K_1 - K_2) \\ K_1(1 + x) + x_{\tilde{t}}(K_2 - K_1) \end{pmatrix} & 0 \leqslant \tilde{t} < \frac{\tau}{2} \\ \begin{pmatrix} K_1(1 + x) + x_{\tilde{t} - \tau/2}(K_2 - K_1) \\ K_2(1 + x) + x_{\tilde{t} - \tau/2}(K_1 - K_2) \end{pmatrix} & \frac{\tau}{2} \leqslant \tilde{t} < \tau. \end{cases} \qquad (34)$$

Here $\tilde{t} \equiv t \mod \tau$, and $x_t \equiv \exp[-(K_1 + K_2)t]$. We use this compact notation since exponentials like x_t are ubiquitous in the following calculations. We remind the reader that $x_{\tau/2} = x$ as this specific term appears quite often. It is easy to verify that this solution is consistent with Eqs. (18) and (19).

The linear correction to the power output is obtained by taking the leading order variation of Eq. (6). We find

$$\delta\Phi = f \int_0^\tau dt' \left[\delta R_{ba}^{(1)} P_a - \delta R_{ab}^{(1)} P_b + \delta R_{ab}^{(2)} P_b - \delta R_{ba}^{(2)} P_a \right.$$
$$\left. + R_{ba}^{(1)}\delta P_a - R_{ab}^{(1)}\delta P_b + R_{ab}^{(2)}\delta P_b - R_{ba}^{(2)}\delta P_a \right].$$
$$(35)$$

To be able to say something useful about the sign of $\delta\Phi$ we need to rewrite this quantity as a time integral over the change of the rates, $\delta R_{ij}(t)$, multiplied by known functions of time. The first four terms in Eq. (35) already have the desired form, but the last four terms do not. To proceed, we first find explicit expressions for the linear corrections to the periodic state. The details are given in Appendix B.

The symmetry of the model and cycle can be used to simplify the calculations. As mentioned above, in the unperturbed solution, the two sites and barriers play the same role at different parts of the cycle. As a result a change in E_a at time $0 < t < \frac{\tau}{2}$ plays the same role as the same change in E_b at time $t + \frac{\tau}{2}$. This means any perturbation in the second half of the cycle has an equivalent counterpart in the first

half. Moreover, in linear order the contributions from different times are additive. It is therefore enough to show that $\delta\Phi$ is negative to all possible small changes of rates in the first half of the cycle. Substituting the value of the unperturbed rates, we find

$$
\delta\Phi = f \int_0^{\frac{\tau}{2}} dt' \big[\delta R_{ba}^{(1)} P_a - \delta R_{ab}^{(1)} P_b + \delta R_{ab}^{(2)} P_b - \delta R_{ba}^{(2)} P_a \big]
$$
$$
+ f(K_1 + K_2) \bigg[\int_0^{\frac{\tau}{2}} dt' \delta P_a(t') - \int_{\frac{\tau}{2}}^{\tau} dt' \delta P_a(t') \bigg]. \quad (36)
$$

By integrating Eq. (B7) from 0 to $\frac{\tau}{2}$, and from $\frac{\tau}{2}$ to τ, one can obtain

$$
(K_1 + K_2) \bigg[\int_0^{\frac{\tau}{2}} dt' \delta P_a(t') - \int_{\frac{\tau}{2}}^{\tau} dt' \delta P_a(t') \bigg]
$$
$$
= 2 \bigg[\delta P_a(0) - \delta P_a\Big(\frac{\tau}{2}\Big) \bigg] + \int_0^{\frac{\tau}{2}} dt' \big[\big(\delta R_{ab}^{(1)} + \delta R_{ab}^{(2)}\big) P_b
$$
$$
- \big(\delta R_{ba}^{(1)} + \delta R_{ba}^{(2)}\big) P_a \big]. \quad (37)
$$

With the help of Eq. (B11), the linear correction for the output can be written as

$$
\delta\Phi = 2f \int_0^{\frac{\tau}{2}} dt' \bigg\{ \bigg[1 - \frac{1}{1+x} e^{-(K_1+K_2)\left[\frac{\tau}{2}-t'\right]} \bigg] \big(\delta R_{ab}^{(2)} P_b - \delta R_{ba}^{(2)} P_a \big)
$$
$$
+ \frac{1}{1+x} e^{-(K_1+K_2)\left[\frac{\tau}{2}-t'\right]} \big(\delta R_{ba}^{(1)} P_a - \delta R_{ab}^{(1)} P_b \big) \bigg\}. \quad (38)
$$

The possible perturbations of the rates are not independent since, for instance, a small change in E_a will affect both $\delta R_{ba}^{(1)}$ and $\delta R_{ba}^{(2)}$. We wish to write the linear correction to the output as a sum over independent terms. It will be convenient to work with the variables $\mathcal{E}_{a,b} = e^{E_{a,b}/T}$ and $\mathcal{B}_{1,2} = e^{-B_{1,2}/T}$. The rates can be expressed in terms of these variables as $R_{ba}^{(1)} = \mathcal{E}_a \mathcal{B}_1 e^{-f\theta/T}$, $R_{ab}^{(1)} = \mathcal{E}_b \mathcal{B}_1 e^{f(1-\theta)/T}$, $R_{ba}^{(2)} = \mathcal{E}_a \mathcal{B}_2 e^{f(1-\theta)/T}$, and $R_{ab}^{(2)} = \mathcal{E}_b \mathcal{B}_2 e^{-f\theta/T}$.

We now focus on perturbations made in the first half of the cycle. $0 \leqslant t < \frac{\tau}{2}$. During the first half of the cycle, $\mathcal{E}_a(t) =$

$\mathcal{E}_{\max} = e^{E_{\max}/T}$ and $\mathcal{E}_b(t) = 1$, and only perturbations with $\delta\mathcal{E}_a(t) \leqslant 0$ and $\delta\mathcal{E}_b(t) \geqslant 0$ are admissible. For the barriers, we have $\mathcal{B}_1(t) = 1$ and $\mathcal{B}_2(t) = 0$ and as a result the perturbations must have $\delta\mathcal{B}_1(t) \leqslant 0$ and $\delta\mathcal{B}_2(t) \geqslant 0$. The linear variation of the rates during the first half of the cycle can the be recast as

$$
\delta R_{ba}^{(1)} = \delta\mathcal{E}_a e^{-f\theta/T} + \delta\mathcal{B}_1 \mathcal{E}_{\max} e^{-f\theta/T} = \delta\mathcal{E}_a K_1/\mathcal{E}_{\max} + \delta\mathcal{B}_1 K_1,
$$
$$
\delta R_{ab}^{(1)} = \delta\mathcal{E}_b e^{f(1-\theta)/T} + \delta\mathcal{B}_1 e^{f(1-\theta)/T} = \delta\mathcal{E}_b K_2 + \delta\mathcal{B}_1 K_2,
$$
$$
\delta R_{ba}^{(2)} = \delta\mathcal{B}_2 K_1 e^{f/T} = \delta\mathcal{B}_2 \mathcal{E}_{\max} K_2,
$$
$$
\delta R_{ab}^{(2)} = \delta\mathcal{B}_2 K_1/\mathcal{E}_{\max}. \quad (39)
$$

Substitution of Eq. (39) allows us to rewrite Eq. (38) in the form

$$
\delta\Phi = 2f \int_0^{\frac{\tau}{2}} dt' [\delta\mathcal{E}_a(t') g_a(t') + \delta\mathcal{E}_b(t') g_b(t')
$$
$$
+ \delta\mathcal{B}_1(t') g_1(t') + \delta\mathcal{B}_2(t') g_2(t')]. \quad (40)
$$

We find that $g_a(t) = \frac{K_1}{(1+x)\mathcal{E}_{\max}} e^{-(K_1+K_2)\left[\frac{\tau}{2}-t\right]} P_a(t) \geqslant 0$. Since $\delta\mathcal{E}_a(t) \leqslant 0$, one sees that small changes in E_a must result in a smaller output. Noting that $g_b(t) = -\frac{K_2}{(1+x)} e^{-(K_1+K_2)\left[\frac{\tau}{2}-t\right]} P_b(t) \leqslant 0$ and that $\delta\mathcal{E}_b \geqslant 0$, we conclude that the same applies for small changes in $E_b(t)$.

The dependence on changes in the barriers is somewhat more complicated. One finds $g_1(t) = \frac{1}{1+x} e^{-(K_1+K_2)\left[\frac{\tau}{2}-t'\right]} \times \{K_1 P_a(t) - K_2 P_b(t)\}$. The term in curly brackets is minimal at $t = \frac{\tau}{2}$, where its value is $(K_1 + K_2)x/(1+x)$. In fact, $K_1 P_a(t) - K_2 P_b(t)$ will reach zero if the system is left to relax to equilibrium with time independent rates. As a result, $K_1 P_a(t) - K_2 P_b(t) \geqslant 0$ for all $0 \leqslant t \leqslant \tau/2$ in the unperturbed solution. We therefore find that $g_1(t) > 0$. Combined with $\delta\mathcal{B}_1(t) \leqslant 0$, we find that reducing the height of the barrier B_1 results in a smaller output.

The remaining term involves the function $g_2(t) = [1 - \frac{1}{1+x} e^{-(K_1+K_2)\left[\frac{\tau}{2}-t\right]}](\frac{K_1}{\mathcal{E}_{\max}} P_b(t) - K_2 \mathcal{E}_{\max} P_a(t))$. The term in the first square brackets is clearly positive. The second term is largest at $t = \frac{\tau}{2}$, where its value is

$$
\frac{K_1}{\mathcal{E}_{\max}} P_b\Big(\frac{\tau}{2}\Big) - K_2 \mathcal{E}_{\max} P_a\Big(\frac{\tau}{2}\Big) = \frac{1}{(K_1 + K_2)(1+x)\mathcal{E}_{\max}} \big[K_1^2 (1 - e^{\frac{2f}{T}}) + x K_1 K_2 (1 - \mathcal{E}_{\max}^2) \big]. \quad (41)
$$

Noting that $f > 0$ and $\mathcal{E}_{\max} > 1$, we find that $g_2(t) < 0$ for $0 \leqslant t < \frac{\tau}{2}$. The allowed perturbations $\delta\mathcal{B}_2(t) \geqslant 0$ can therefore only decrease the output. We just checked that all admissible small changes to the rates always decrease the output.

The conclusion from the preceding calculations is that the cycles studied in Sec. V locally maximize the output with respect to small changes in the driving cycle. This should not be taken as a rigorous proof that such cycles are indeed the optimal solution. The reason is that we have not shown that the cycle is also maximal with respect to so-called needle perturbations, which allow for large changes of parameters for an infinitesimal time. Such perturbations are commonly studied in optimal control [34]. In the next section, a numer-

ical approach will suggest that this solution is unstable to changes in the period τ, which can be interpreted as a needle perturbation. Nevertheless, the same numerical results show that the optimal cycle can be understood in terms of cycles of the type studied here by comparing cycles with different periods.

VII. NUMERICAL MAXIMIZATION USING A GENETIC ALGORITHM

We complement the analytical arguments given above with a numerical approach that searches for the optimal solution in an completely different way. Finding out that two independent approaches lead to the same results will greatly strengthen our confidence in the validity of the results.

A. A genetic algorithm

Numerically searching for the driving protocol that maximizes the output is challenging due to the need to explore the space of four periodic functions, $E_{a,b}(t)$ and $B_{1,2}(t)$. A gradient-based search is likely to wander around in nearly flat regions of the space and then be trapped in some local maximum. Instead, we used an approach that is based on a genetic algorithm [81]. The term genetic algorithm is used here to describe a heuristic method of searching for a maximum that is inspired by the way that populations of living organisms evolve to improve their fitness. In evolution, a phenotype relevant for survival can be present in a generation of a population. The phenotype results from an expression of genes and genetic variation results in variability of phenotypes. The survivors of natural selection then constitute the next generation. This population includes members with random minor changes due to mutations. The process repeats itself and the fitness of the entire population improves because, although most individual changes are detrimental, beneficial changes are more likely to be propagated to the following generations. Our genetic algorithm operates similarly, with the output as the phenotype, and the time dependence of the energies and barriers as the genetic code.

Specifically, the genetic code of a member of the population is defined as the values of $E_a(t)$, $E_b(t)$, $B_1(t)$, and $B_2(t)$ during the cycle. In practice, the cycle was divided into N time segments, $[\tau i/N, \tau(i+1)/N)$, with $i = 0, 1, 2, \ldots, N-1$. We used $\tau = 2\pi/6$, and $N = 128$ in all the results presented below. In each time segment, the energies and barriers were taken to be constant during the segment. The driving protocol is then identified by recording the energies and barriers in each of the segments, $E_{a,b}(t_i)$ and $B_{1,2}(t_i)$. These 512 values define the genetic code of each driving cycle. For practical reasons, we enforced a maximal value of $B_{\max} = 10$ to the various barriers. The maximal energy was chosen to be $E_{\max} = 2$.

The selection criterion is, naturally, based on the maximization the output ϕ of the system, as defined in Sec. III. It can be calculated efficiently as described in the following. In each of the time segments, one can generalize the spectral decomposition presented in Appendix A to a rate matrix with arbitrary, but time-independent, rates. The resulting propagator for the ith time step is

$$\mathbf{U}_i = \frac{1}{\left|\lambda_2^{(i-1)}\right|} \begin{pmatrix} R_{ab}^{(i-1)} + e^{\lambda_2^{(i-1)}(t_i-t_{i-1})}R_{ba}^{(i-1)} & R_{ab}^{(i-1)}[1 - e^{\lambda_2^{(i-1)}(t_i-t_{i-1})}] \\ R_{ba}^{(i-1)}[1 - e^{\lambda_2^{(i-1)}(t_i-t_{i-1})}] & R_{ba}^{(i-1)} + e^{\lambda_2^{(i-1)}(t_i-t_{i-1})}R_{ab}^{(i-1)} \end{pmatrix}. \tag{42}$$

Here $R_{ab}^{(i)} \equiv R_{ab}^{(1)}(t_i) + R_{ab}^{(2)}(t_i)$, $R_{ba}^{(i)} \equiv R_{ba}^{(1)}(t_i) + R_{ba}^{(2)}(t_i)$, and $\lambda_2^{(i)} = -R_{ab}^{(i)} - R_{ba}^{(i)}$. The propagator of a complete cycle, $\mathbf{U} = \prod_i \mathbf{U}_i$, can then be used to find the periodic solution satisfying $\vec{P}(\tau) = \mathbf{U}\vec{P}(0) = \vec{P}(0)$.

Once the periodic solution is found, the output of the cycle is calculated by adding contributions from each time step. In the ith time step, $\mathbf{U}_i$ can be used to propagate the probabilities $P_{a,b}(t_{i-1})$ to $P_{a,b}(t_i)$. Then the contribution of this time step to the output of the stochastic pump is calculated using

$$\delta\phi_i = \frac{2f}{\left|\lambda_2^{(i-1)}\right|}(t_i - t_{i-1})\left[R_{ba}^{(1)}(t_{i-1})R_{ab}^{(2)}(t_{i-1}) - R_{ba}^{(2)}(t_{i-1})R_{ab}^{(1)}(t_{i-1})\right]$$

$$+ \frac{f}{\left|\lambda_2^{(i-1)}\right|}\left[R_{ba}^{(1)}(t_{i-1}) + R_{ab}^{(1)}(t_{i-1}) - R_{ba}^{(2)}(t_{i-1}) - R_{ab}^{(2)}(t_{i-1})\right]\{P_b(t_i) - P_b(t_{i-1})\}. \tag{43}$$

A derivation of Eq. (43) can be found in Appendix C. Summation of the contributions from all the time steps results in the output of the whole cycle. Numerical calculations that are based on piecewise constant parameters turn out to be fast and reliable, since there is no need for naive numerical integration that requires subdivision of the time segments to smaller time steps.

A genetic algorithm that is built upon those calculations is then applied. A population consisting of 200 different driving protocols is generated and constitutes the first generation. Initially, the energies were drawn randomly while the barriers were set to 1. This population is then subjected to an evolution is which new generations replace old ones by a process of mutations and selection. Our algorithm used several types of mutations and other genetic variations to generate new driving protocols:

(1) In small mutations, one of the parameters, i.e., $B_2(t_i)$, was chosen at random. This value was then modified by adding a random number taken from the range $\pm 2.5E_{\max}/100$.

The new value was truncated if it exceeded the allowed range for this parameter.

(2) Large mutations are similar, but the change in the parameter could be as large as $\pm 0.5E_{\max}$.

(3) Group mutations are similar to small mutations, but the change is applied to all the values of the same parameter in a small time segment (one to five time steps).

(4) A replication is made by picking a time t_i at random and then copying the values of $E_{a,b}(t_i)$ and $B_{1,2}(t_i)$ onto their counterparts at time t_{i+1}.

(5) An inversion mutation is created by picking a time t_i and a time segment at random. The segment can have any length between one time step to half of the cycle. For all the parameters in this time segment, one applies the inversion $E \to E_{\max} - E$ and, similarly, $B \to B_{\max} - B$.

(6) Barrier-lowering mutations were used to help some systems escape local maximums. An initial time and segment length (between $\tau/128$ and $\tau/2$) were chosen at random. Then one of the energies (namely, a or b) and one of the barriers
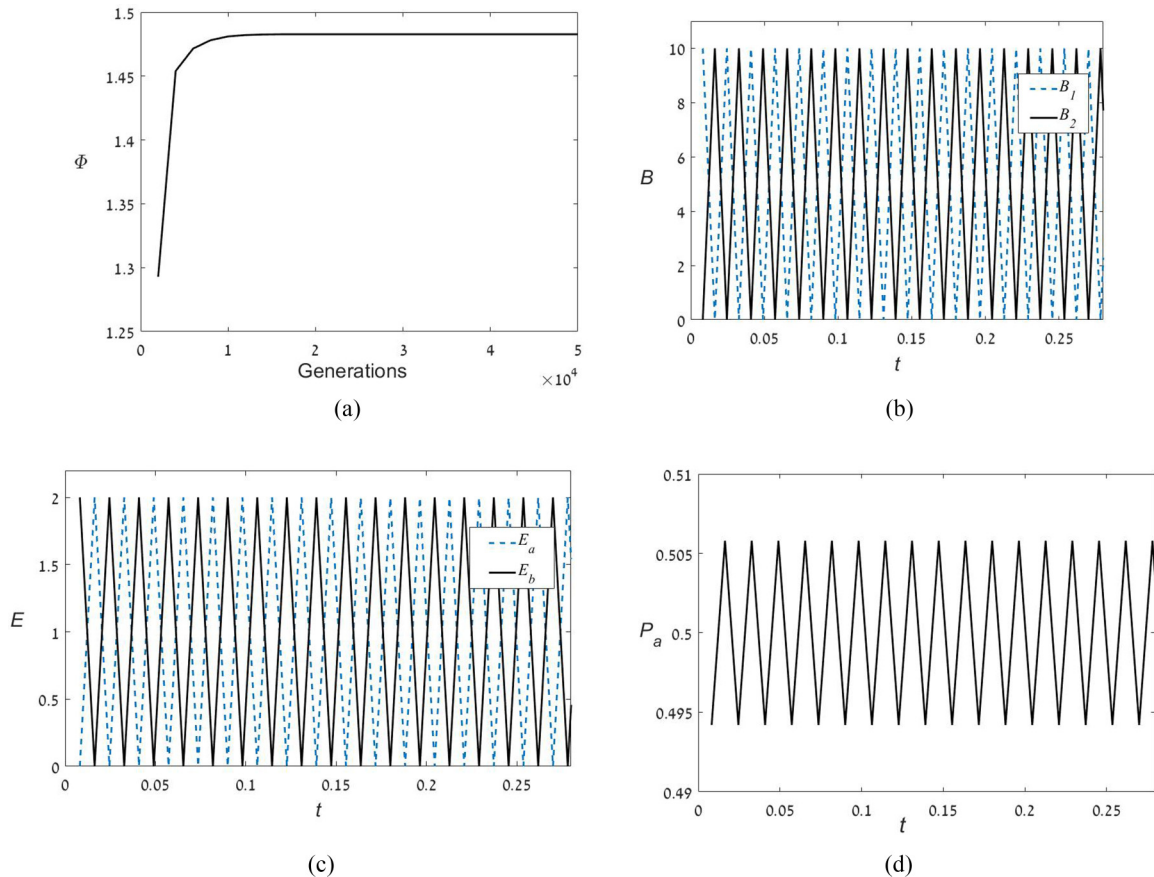
FIG. 2. Results of the genetic algorithm: (a) Output as a function of the number of generations. (b) The time dependence of barriers in the cycle with highest output. (c) Time dependence of the site energies in this cycle. (d) The time dependence of the probability, $P_a(t)$. To avoid clutter, only the first quarter or so of the external period τ are shown in panels (b)–(d).

(1 or 2) were chosen randomly. The values of the barrier [e.g., $B_2(t_i)$] in all times during the segment were set to $E_{max}/10$, whereas values of the energy in the segment were set to a time-independent random value (between 0 and E_{max}).

(7) In a recombination, two new cycles are created from an existing pair of cycles by exchanging the values of the parameters between two equal length segments. Both the initial times as well as the length of the segment (between one step and $\tau/2$) were chosen randomly.

A new generation was created from an existing one using the following scheme. The ten members with the highest output were passed to the new generation without any modifications. Twenty members were created by applying small mutations to these ten members. Similarly, ten members were the result of group mutations. Twenty members of the new generations were created by choosing at random a member of the current generation and applying a large mutation. Another ten members were created using a similar process with replication, ten members underwent barrier lowering, and a further 20 had inversion mutations. Finally, the remaining 100 members were generated by randomly choosing 50 pairs of members of the current generation and using recombination. The resulting new generation thus includes a population of 200, the same as its predecessor. This process leads to generations that are built from small variations to the members with the highest output and a variety of members with

larger changes to their genetic code, thereby maintaining a diverse population. The algorithm progresses between successive generations until it seems that the maximal output observed in each generation saturates. One then hopes that the cycle with the maximal output is indeed the globally optimal solution.

B. Results

Figure 2(a) depicts the variation of the maximal output with different generations. One can see that for a while the output tends to increase with progressing generations. The figure is smoothed by only including points taken every 2000 generations. After a certain number of generations, the maximal output saturates, suggesting convergence to either a deep local or the global maximal output cycle.

Figures 2(b) and 2(c) show the time dependence of the energies and barriers of the optimal cycle (according to the genetic algorithm). For clarity, only the first quarter of the cycle is depicted, since it is hard to distinguish different lines when the full period is shown. At each time step, the value of the parameters match one of the two sets of parameters that were identified in the cycles studied in Sec. V. To be precise, we find either $E_a = 2, E_b = 0, B_1 = 0, B_2 = 10$ or $E_a = 0, E_b = 2, B_1 = 10, B_2 = 0$. Crucially, the solution that the algorithm found alternates between the two sets of parameters

at each time step. Figure 2(d) depicts the time evolution of the probability $P_a(t)$ in the optimal cycle. The rapid switching of parameters keeps this probability fairly close to its symmetric value $P_a = P_b = 1/2$.

C. Comparison with the analytical approach

At first, the numerical candidate for an optimal solution may seem at odds with the locally optimal solutions studied in Secs. V and VI. However, a careful consideration reveals that our discussion there assumed that the period τ of the cycle was fixed, whereas we actually demanded that $E_a(t) = E_a(t + \tau)$, etc. This is consistent with cycles with a period of τ/n for any positive integer n, as well as other, suboptimal combinations of cycles with smaller periods. For cycles with period τ/n, the output accumulated after a time τ is

$$\Phi_n(\tau) = n \frac{2f(K_1 - K_2)}{K_1 + K_2} \frac{1 - \exp\left[-(K_1 + K_2)\frac{\tau}{2n}\right]}{1 + \exp\left[-(K_1 + K_2)\frac{\tau}{2n}\right]}. \quad (44)$$

$\Phi_n(\tau)$ increases with n, meaning that the maximal output is obtained in the limit of vanishing cycle period. The output accumulated after a time τ is therefore bounded by

$$\Phi^* = \lim_{n \to \infty} \Phi_n(\tau) = \frac{f\tau}{2}(K_1 - K_2). \quad (45)$$

This observation fits well with the numerical results. The numerical algorithm converged to the solution with the smallest cycle period that was available to it. It suggests that the two-site stochastic pump is operated at maximum output when a singular driving protocol is used. In this singular cycle, the pump alternates between the two sets of parameters at an infinite rate, meaning that one cannot assign a definite value for $E_{a,b}(t)$ and $B_{1,2}(t)$. The resulting maximal power output is given by

$$\dot{\Phi}^* = \frac{f}{2} e^{-\frac{f\theta}{T}} [e^{\frac{E_{\max}}{T}} - e^{\frac{f}{T}}], \quad (46)$$

which can be used to numerically calculate the resisting force f that would increase the power further. In the linear response regime, one finds $f^* = \frac{E_{\max}}{2}$, as expected.

Solutions that involve infinitely fast switching of the external driving are known in the field of control theory [76,77]. The terms chattering and sliding control are used to describe various control solutions with this property. The combination of numerical results and the analytical arguments given here suggest that a solution exhibiting such rapid switching is the optimal solution for the problem studied here.

VIII. COMPARISON OF REGULARIZED ANALYTICAL AND NUMERICAL OPTIMAL SOLUTIONS

A possible problem with the results presented in the previous section is that the numerically obtained optimal solution was restricted by the discrete times steps we used. One may be worried that the resulting driving cycle is a numerical artifact rather than the best possible approximation for the unconstrained optimal solution. It is therefore desirable to test the genetic algorithm in situations where its convergence is less affected by this specific externally placed restriction. In this section, we chose to modify the criterion for optimiza-

tion to penalize too-frequent parameter switching events. The modified optimal solutions are regularized to exhibit finite periods.

In the genetic algorithm, we apply this scheme by defining a cost that includes a (typically small) penalty to changes in site energies:

$$C(\epsilon, \tau) \equiv \Phi(\tau) - \epsilon \sum_{i=1}^{N} \sum_{\alpha=a,b} |E_\alpha(t_{i+1}) - E_\alpha(t_i)|. \quad (47)$$

Here $\Phi(\tau)$ is the accumulated output up to time τ. We then use the genetic algorithm to look for the solutions that maximize this cost. For small values of ϵ, we expect that this penalty will not drastically change the nature of the solutions, in the sense that they still switch between the same two sets of variables, albeit at a finite rate.

Figure 3 depicts the results of the algorithm for $\epsilon = 0.0044$. Figure 3(a) shows the maximal value of the cost for different generations. The curve is smoothed by only including points spaced by 2000 generations. The results in the panel show convergence to a (global or local) maximum. Figures 3(b)–3(d) present the resulting optimal solution. One sees that this solution alternates between the same two sets of parameters as its counterpart with $\epsilon = 0$. However, it does so at a finite rate that is not constrained by the lattice of time points used. The solution completes four full cycles in the externally mandated period τ. The longer period of the cycle result in a larger variation of the probability $P_a(t)$, as can be seen by comparing Fig. 2(d) with Fig. 3(d).

A simple, but approximate, analytical description of the way that the parameter ϵ affects the period of the optimal solution can be made based on the properties of the cycles studied in Sec. V. For small ϵ, it is reasonable to expect that the optimal solution is composed of n cycles with period τ/n, so in each period E_a and E_b switch twice between 0 and $E_{\max}$ (at different times). The barriers behave similarly. The accumulated output is therefore given by Eq. (44). The penalty due to changes in energy is then $-4n\epsilon E_{\max}$. One then needs to consider the cost

$$C(\epsilon, \tau) = \phi_n(\tau) - 4n\epsilon E_{\max}. \quad (48)$$

TABLE I. Comparison of the predicted and observed number of cycles completed in $t = \tau$ as a function of ϵ. The number of cycles is controlled by a cost of changing energies, parametrized by ϵ. $\tilde{n}$ is the number of compete cycles that maximizes the cost Eq. (48). n^* is found by treating this number is being continuous rather than integer. Finally, n_{obs} is the number of cycles found in the solutions identified by the genetic algorithm.

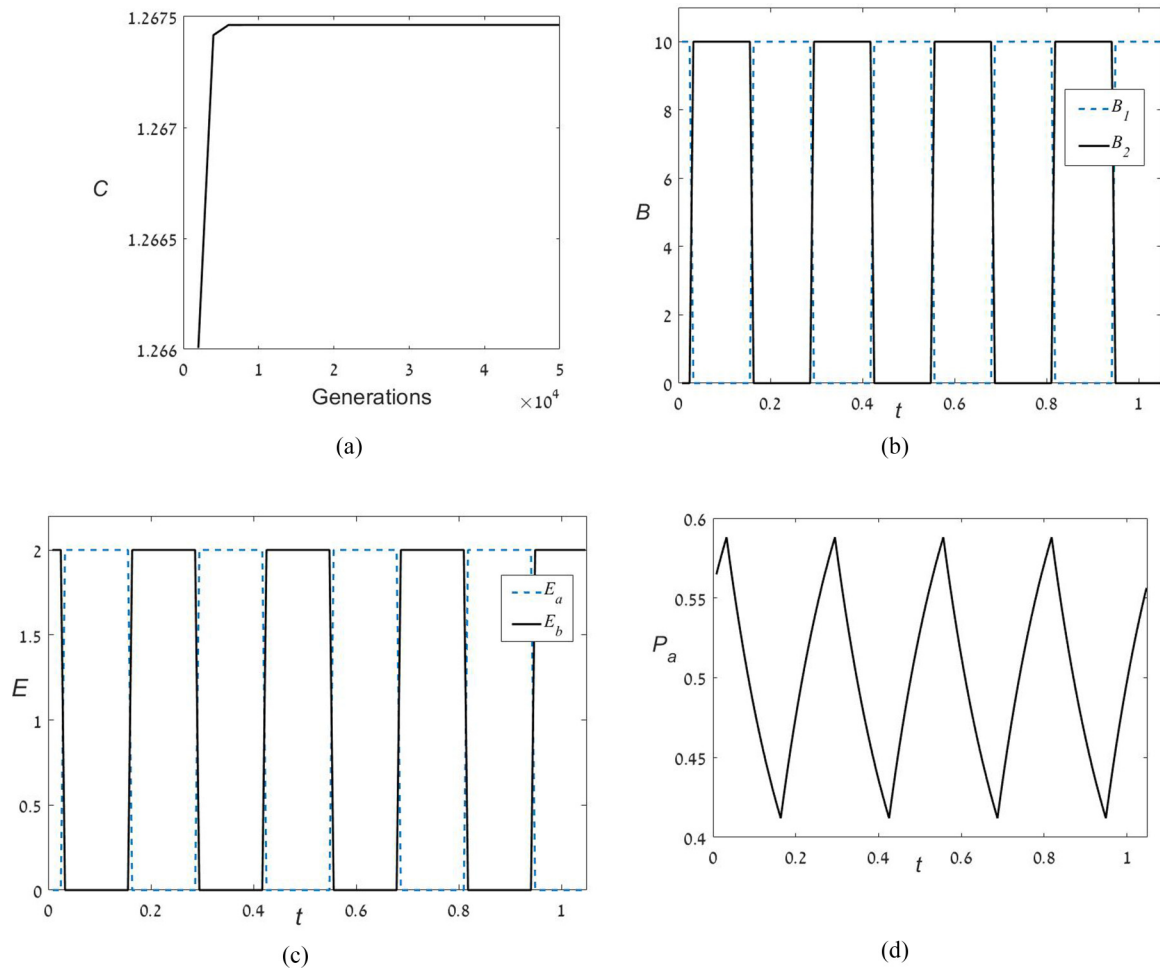| ϵ	n^*	$\tilde{n}$	n_{obs}
1.21×10^{-6}	64.070	64	64
9.70×10^{-6}	31.997	32	32
3.39×10^{-5}	21.069	21	21
7.70×10^{-5}	16.008	16	16
6.00×10^{-4}	8.011	8	8
1.38×10^{-3}	6.019	6	6
4.40×10^{-3}	3.997	4	4
9.55×10^{-3}	2.994	3	3
2.51×10^{-2}	2.004	2	2

FIG. 3. Results of the genetic algorithm for optimization with respect to the cost (47): (a) The cost as a function of the number of generations; (b) The time dependence of barriers in the converged solution; (c) Time dependence of the site energies in the solution; and, (d) The time dependence of the probability to reside in site a.

The number of actual cycles that is expected, $\tilde{n}$, is the one that maximizes Eq. (48) for given ϵ and τ. It can be found by comparing the value of the cost for $n = 1, 2, 3, \ldots$ or be approximated by finding the (noninteger) n^* that satisfies $\frac{\partial C}{\partial n}\big|_{n=n^*} = 0$. One then expects the genetic algorithm to converge to a solution with this number of periods. This is indeed what we observed for the cases we tested. For instance, for $\epsilon = 0.044$ the cost is maximized for $n^* \simeq \tilde{n} = 4$, and the results depicted in Fig. 3 indeed show a solution with four complete cycles. Table I compares the expected and observed number of cycles for several values of ϵ. Excellent agreement is found between the analytical prediction and the results of the genetic algorithm in all cases.

We note that occasionally the algorithm may converge to a solution with either one additional or one missing cycle. Such solutions can serve as local maxima that trap the genetic algorithm. While these solutions have a lower cost then the one with the correct number of cycles, the genetic algorithm sometimes finds it hard to escape from their neighborhood. Nevertheless, comparison of several independent runs of the algorithm is quite likely to find the correct maximum.

Figure 4 shows a comparison of the expected and observed output as a function of the parameter ϵ. The curves correspond

to the the analytically calculated output. The blue dashed curve is obtained by substituting n^* in Eq. (44). The solid black curve is obtained by substituting the integer number
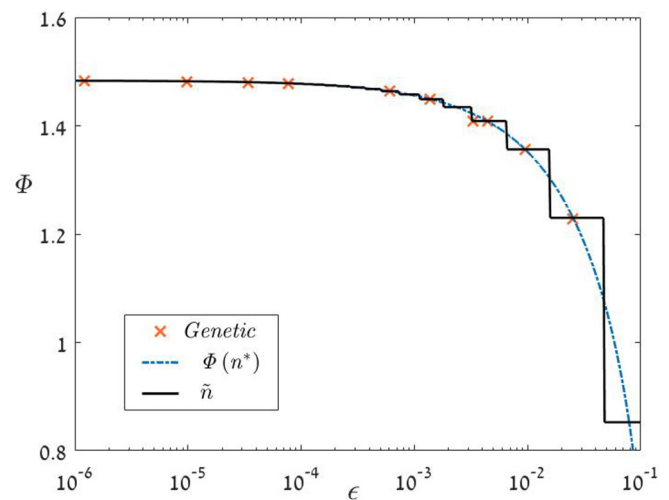

FIG. 4. Comparison of the output of the optimal solutions found by the genetic algorithm with the corresponding analytical estimates.

of cycle that maximizes Eq. (48), $\tilde{n}$, in Eq. (44). Finally, the red crosses denotes the output of the solution obtained by the genetic algorithm.

The results depicted in Table I and Fig. 4 demonstrate that the analytical estimate described above matches the results of the genetic algorithm. Both the results depicted in Figs. 3 and 4 show that the optimal solutions of the model are indeed built out of the locally optimal cycles studied in Sec. V. As ϵ decreases, so does the period of the actual cycles that appear in the optimal solution. This reinforces the expectation that in the limit $\epsilon \to 0$ the optimal solution will exhibit singular behavior with an infinite rate of switching between the two sets of site energies and transition barriers. After all, this singular optimal solution matches the trends seen in both the numerical and analytical approaches used here.

IX. DISCUSSION

We have studied the driving cycles that maximize the power output of a two-site stochastic pump. A combination of an analytical approach and a numerical optimization based on a genetic algorithm, suggests that the optimal driving protocol switches between two system configurations in which the site energies and barriers are either maximal or minimal. Surprisingly, the optimal driving protocol turns out to be singular, switching between the two configurations at an infinite rate. In this optimal solution, the probabilities to reside in the two sites stay arbitrarily close to $\frac{1}{2}$. Yet, in each infinitesimally short time segment, an infinitesimal amount of probability if pushed from one site to the other. Over finite times, these add up to create a finite output.

This optimal solution can be regularized by introducing an additional cost to changes in site energies. We find that this results in optimal cycles with finite periods. Importantly, both the numerical and analytical approaches predict the same cycles. This agreement strengthens the conclusion regarding the singular behavior of the optimal solutions when the cost assigned to energy changes approaches zero.

One may ask if we should have anticipated such singular optimal solutions and how typical they are. In hindsight, it seems that such solutions should be quite typical in overdamped systems, as long as the period is not fixed externally. Consider a similar model with several sites. For time-independent rates, the system follows an evolution that qualitatively exhibits a relaxation toward a steady state. This relaxation is often described as a sum of several exponentially decaying terms. A cycle is then typically composed of a finite chain of such decays. Note that we assumed that any candidate for optimal solution is of the bang-bang type, composed of a series of segments in which the rates are fixed. The probability to be in one of the sites will heuristically look like the curve depicted in Fig. 5. One can expect the contribution to the output, which is generated by fluxes entering and leaving the site, to be roughly proportional to the overall change of probability in the site, ΔP_i. The exact details depend on the precise configuration of allowed transitions, resisting forces, the site energies, and the barriers. By the nature of the exponential relaxation, the magnitude of the probability variation ΔP_i depends nonlinearly on the time spent in each segment of the cycle. Crucially, doubling the time will not result in a
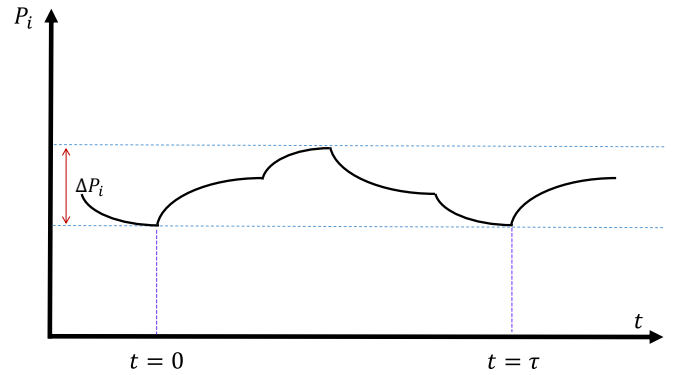

FIG. 5. Heuristic depiction of a cycle in a more general stochastic pump. The time dependence of the probability to be in site i is shown. The cycle is composed of four different segments. In each segment, the rates are assumed to be constant and the dynamics exhibit a typical exponential relaxation toward a limiting state.

doubling of ΔP_i. For instance, in the two-site model studied here $\Delta P_i \propto \tanh(\frac{K_1+K_2}{4}\tau)$, see Eq. (21). But $\tanh(\frac{K_1+K_2}{4}\tau) \leqslant \frac{K_1+K_2}{4}\tau$, meaning that the rate of accumulating output is maximized in the limit $\tau \to 0$, where the inequality is saturated. This qualitative argument suggests that such behavior should be quite typical for systems whose dynamics decay exponentially toward a steady state, although one cannot exclude some ways of tuning systems to achieve faster than expected relaxation [82]. All this means that singular optimal solutions with infinite rate of switching should be quite typical if the problem is set up so infinitesimal cycle periods are allowed and make physical sense.

Finally, it is worth commenting on the possible implications of the results to the design and operation of artificial molecular machines. Indeed, an artificial molecular motor whose structure is similar to the one studied here has been realized [80]. Furthermore, models of stochastic pumps have been used to theoretically describe some experimental realizations of molecular machines [73]. Such models are based on an assumption of separation of timescales. Specifically, one assumes that the external changes used to drive the molecular machines are faster compared to the time it takes the molecular machine to change its (mechanical) configuration. Furthermore, it is assumed that the molecule reaches some local equilibrium on a short timescale, allowing one to describe its conformation changes as a memoryless (Markov) process. Under such assumptions, the driving cycles used in several experiments are similar to the cycles studied in Sec. V. They are built of relatively fast external manipulations and time segments in which the system is left to evolve under constant conditions. One may wonder if such driving protocols are optimal. Should one attempt to develop more sophisticated, explicitly time-dependent driving mechanisms?

The results shown above suggest that such piecewise driving protocols can be locally optimal and that there is no reason to expect any gain from developing a driving protocol with more gradual time variation of external parameters. The singular driving protocol which maximizes the power output breaks all the assumptions about separation of timescales described above. However, we point out that it is not realistic

to expect to be able to switch between configurations with an infinite rate. Moreover, most of the gain in power output is obtained when the switching is comparable to the relaxation rate. For instance, using $\tau = \frac{1}{2(K_1 + K_2)}$ in Eq. (21) gives about 77% of the maximal output Eq. (45). This means that most of the output can be achieved under conditions where models of the type studied here are valid. The results presented above then suggest driving artificial molecular machines by making sudden switches between configurations at a rate that is several times faster than the typical relaxation rate of the system.

The example studied here was of a particularly simple two-site system. It will be interesting to see how the results generalize to other, less restricted, systems. Is there a qualitative change if one breaks the symmetry between the two sites, for instance, by allowing different maximal energies? What is the optimal cycle in a system of n sites linked by a cycle of transitions? How does the optimal driving protocol look if there are two coupled cycles? Is it better to mainly drive transitions in the shorter cycle? And what happens if the maximal barrier is finite and therefore one cannot fully isolate one cycle? Such questions are left for future work.

ACKNOWLEDGMENTS

APPENDIX A: SPECTRAL DECOMPOSITION OF THE RATE MATRIX

The cycle studied in Sec. V was characterized by rate matrices that were piecewise constant in time. In the first half of the cycle, we had

$$\mathbf{R}_1 = \begin{pmatrix} -K_1 & K_2 \\ K_1 & -K_2 \end{pmatrix}. \tag{A1}$$

In the following, we find the spectral decomposition of $\mathbf{R}_1$ and use it to construct the propagator for the part of the cycle where $\mathbf{R}_1$ is the rate matrix.

We start by finding the eigenvalues of $\mathbf{R}_1$. The dynamics generated by the master equation conserve probability. As a result, one of the eigenvalues of $\mathbf{R}_1$ must be $\lambda_1 = 0$. The other eigenvalue can be obtained from the trace of $\mathbf{R}_1$, namely, $\lambda_2 = -(K_1 + K_2)$.

The eigenvectors associated with the eigenvalue $\lambda_1 = 0$ have a simple physical interpretation. The right eigenvector is the equilibrium probability density:

$$v_1 = \frac{1}{K_1 + K_2} \begin{pmatrix} K_2 \\ K_1 \end{pmatrix}. \tag{A2}$$

The left eigenvector is associated with the summation over all probabilities needed for normalization:

$$w_1 = \begin{pmatrix} 1 \\ 1 \end{pmatrix}. \tag{A3}$$

The two remaining eigenvectors can be found from the demand that they satisfy biorthogonality relations. Specifically,

$w_2^T \cdot v_1 = 0$ and $w_1^T \cdot v_2 = 0$. One finds

$$v_2 = \begin{pmatrix} 1 \\ -1 \end{pmatrix} \tag{A4}$$

and

$$w_2 = \frac{1}{K_1 + K_2} \begin{pmatrix} K_1 \\ -K_2 \end{pmatrix}. \tag{A5}$$

Once all the eigenvectors and eigenvalues are known, the transition rate matrix $\mathbf{R}_1$ can be rewritten as

$$\mathbf{R}_1 = \lambda_1 v_1 \otimes w_1 + \lambda_2 v_2 \otimes w_2. \tag{A6}$$

Here $\otimes$ is the outer product between two vectors, given by $v \otimes w = v w^T$.

The spectral decomposition Eq. (A6) is useful because it allows us to calculate the exponential of the matrix, namely,

$$\exp[\mathbf{R}_1 t] = e^{\lambda_1 t} v_1 \otimes w_1 + e^{\lambda_2 t} v_2 \otimes w_2$$

$$= \frac{1}{K_1 + K_2} \begin{pmatrix} K_2 & K_2 \\ K_1 & K_1 \end{pmatrix} - \frac{e^{-(K_1 + K_2)t}}{K_1 + K_2} \mathbf{R}_1. \tag{A7}$$

Substitution of $t = \frac{\tau}{2}$ results in Eq. (13).

In the second half of the cycle, the transition rate matrix is given by Eq. (14). It is easy to see that one can use the results given above also for the second half of the cycle as long as one replaces K_1 and K_2.

APPENDIX B: LINEAR RESPONSE CORRECTION TO THE PERIODIC STATE

In the linear response approximation the correction to the probability distribution satisfies the inhomogeneous equation:

$$\frac{d\delta \vec{P}}{dt} = \mathbf{R}_0(t) \delta \vec{P}(t) + \delta \mathbf{R}(t) \vec{P}. \tag{B1}$$

This equation has the following formal solution:

$$\delta \vec{P}(t) = \int_{-\infty}^{t} dt' \, \mathbf{U}_0(t, t') \delta \mathbf{R}(t') \vec{P}(t'), \tag{B2}$$

where the lower limit of integration has been set so the solution is indeed periodic in time. $\mathbf{U}_0(t, t')$ is the propagator of the unperturbed dynamics. It satisfies

$$\frac{d\mathbf{U}_0(t, t')}{dt} = \mathbf{R}_0(t) \mathbf{U}_0(t, t'), \tag{B3}$$

with the initial condition $\mathbf{U}_0(t, t) = \mathbb{I}$.

For the two-site model, the structure of the transition rate matrix means that

$$\delta \mathbf{R}(t) \vec{P}(t) = h(t) \begin{pmatrix} 1 \\ -1 \end{pmatrix}, \tag{B4}$$

where $h(t) = [(\delta R_{ab}^{(1)} + \delta R_{ab}^{(2)}) P_b - (\delta R_{ba}^{(1)} + \delta R_{ba}^{(2)}) P_a]$. Crucially, $\begin{pmatrix} 1 \\ -1 \end{pmatrix}$ is a right eigenvector of the unperturbed transition rate matrix at all times during the cycle. The corresponding eigenvalue is $\lambda_2 = -(K_1 + K_2)$. As a result,

$$\mathbf{U}_0(t, t') \begin{pmatrix} 1 \\ -1 \end{pmatrix} = x_{t-t'} \begin{pmatrix} 1 \\ -1 \end{pmatrix}. \tag{B5}$$

Subsitution of Eqs. (B4) and (B5) into Eq. (B2) gives a simple explicit expression for the linear correction to the asymptotic periodic state:

$$\delta\vec{P}(t) = \int_{-\infty}^{t} dt' x_{t-t'} h(t') \begin{pmatrix} 1 \\ -1 \end{pmatrix}. \qquad (B6)$$

We note that Eq. (B6) means that δP_a is the solution of the scalar equation,

$$\frac{d\delta P_a}{dt} = -(K_1 + K_2)\delta P_a + h(t), \qquad (B7)$$

which will be used in the following.

The periodicity of $\delta\vec{P}(t)$ is ensured by the one of $h(t)$ and the simple exponential structure of x_t. This can be made evident by dividing the integral:

$$\delta\vec{P}(t) = \begin{pmatrix} 1 \\ -1 \end{pmatrix} \left[\int_{t-\tau}^{t} dt' x_{t-t'} h(t') + \int_{t-2\tau}^{t-\tau} dt' x_{t-t'} h(t') \right.$$
$$\left. + \int_{t-3\tau}^{t-2\tau} dt' x_{t-t'} h(t') + \cdots \right]. \qquad (B8)$$

Using changes of variables of the form $t_i = t' + i\tau$ allows us to bring all the integrals in the series back to the same domain of integration. A straightforward calculation results in

$$\delta\vec{P}(t) = \begin{pmatrix} 1 \\ -1 \end{pmatrix} \int_{t-\tau}^{t} dt' x_{t-t'} h(t') [1 + x^2 + x^4 + \cdots]$$
$$= \frac{1}{1-x^2} \int_{t-\tau}^{t} dt' x_{t-t'} h(t') \begin{pmatrix} 1 \\ -1 \end{pmatrix}. \qquad (B9)$$

This explicitly periodic expression for the correction to the periodic state, $\delta\vec{P}(t)$, is helpful in calculating the linear response correction to the power output.

Finally, some of the calculations done in the main text also require an expression for the difference $\delta P_a(\frac{\tau}{2}) - \delta P_a(0)$. Equation (B9) allows us to write

$$\delta P_a\left(\frac{\tau}{2}\right) - \delta P_a(0)$$
$$= \frac{1}{1-x^2} \left[\int_{-\frac{\tau}{2}}^{\frac{\tau}{2}} dt' x_{\frac{\tau}{2}-t'} h(t') - \int_{0}^{\tau} dt' x_{\tau-t'} h(t') \right], \quad (B10)$$

where in the last term we used $\delta P_a(0) = \delta P_a(\tau)$. With the help of the periodicity of $h(t)$, this expression can be rewritten in terms of integrals that are limited to the range $0 \leqslant t' \leqslant \tau$. We find

$$\delta P_a\left(\frac{\tau}{2}\right) - \delta P_a(0)$$
$$= \frac{1}{1+x} \left[\int_{0}^{\frac{\tau}{2}} dt' x_{\frac{\tau}{2}-t'} h(t') - \int_{\frac{\tau}{2}}^{\tau} dt' x_{\tau-t'} h(t') \right]. \quad (B11)$$

APPENDIX C: DERIVATION OF EQ. (43)

To derive Eq. (43), we note that the simple structure of the system allows us to obtain several algebraic relations between the integrated probability fluxes:

$$\phi_{\alpha\beta}^{(j)} \equiv \int_{t}^{t+\Delta t} dt' R_{\alpha\beta}^{(j)} P_{\beta}(t'). \qquad (C1)$$

For time-independent rates, there are enough such relations to solve for the fluxes and use them to calculate the output that has accumulated between t and $t + \Delta t$. Indeed, from the definition of the output it is clear that it can be recast as

$$\delta\Phi = \Phi(t + \Delta t) - \Phi(t) = f\left[\phi_{ba}^{(1)} - \phi_{ab}^{(1)} - \phi_{ba}^{(2)} + \phi_{ab}^{(2)}\right]. \qquad (C2)$$

It is straightforward to relate the change in probabilities to a linear combination of the fluxes:

$$P_a(t + \Delta t) - P_a(t) = P_b(t) - P_b(t + \Delta t)$$
$$= \phi_{ba}^{(1)} + \phi_{ba}^{(2)} - \phi_{ab}^{(1)} - \phi_{ab}^{(2)}. \qquad (C3)$$

For time-independent transition rates, one also finds

$$\frac{\phi_{ba}^{(1)}}{\phi_{ba}^{(2)}} = \frac{R_{ba}^{(1)}}{R_{ba}^{(2)}} \qquad (C4)$$

and

$$\frac{\phi_{ab}^{(1)}}{\phi_{ab}^{(2)}} = \frac{R_{ab}^{(1)}}{R_{ab}^{(2)}}. \qquad (C5)$$

Finally, one can use conservation of probability $P_b(t) + P_a(t) = 1$ to write, e.g.,

$$\frac{\phi_{ab}^{(1)}}{R_{ab}^{(1)}} + \frac{\phi_{ba}^{(2)}}{R_{ba}^{(2)}} = \Delta t. \qquad (C6)$$

Equations (C3)–(C6) can be solved to give

$$\phi_{ab}^{(1)} = -\frac{1}{|\lambda_2|} R_{ab}^{(1)} \Delta P_b + \frac{1}{|\lambda_2|} (R_{ba}^{(1)} + R_{ba}^{(2)}) R_{ab}^{(1)} \Delta t,$$

$$\phi_{ba}^{(1)} = +\frac{1}{|\lambda_2|} R_{ba}^{(1)} \Delta P_b + \frac{1}{|\lambda_2|} (R_{ab}^{(1)} + R_{ab}^{(2)}) R_{ba}^{(1)} \Delta t,$$

$$\phi_{ab}^{(2)} = -\frac{1}{|\lambda_2|} R_{ab}^{(2)} \Delta P_b + \frac{1}{|\lambda_2|} (R_{ba}^{(1)} + R_{ba}^{(2)}) R_{ab}^{(2)} \Delta t,$$

$$\phi_{ba}^{(2)} = +\frac{1}{|\lambda_2|} R_{ba}^{(2)} \Delta P_b + \frac{1}{|\lambda_2|} (R_{ab}^{(1)} + R_{ab}^{(2)}) R_{ba}^{(2)} \Delta t. \quad (C7)$$

As before, the eigenvalue associated with the relaxation rate is $\lambda_2 = -R_{ab}^{(1)} - R_{ab}^{(2)} - R_{ba}^{(1)} - R_{ba}^{(2)}$. Substitution of Eqs. (C7) in (C2) leads to Eq. (43).

[1] H. B. Callen, *Thermodynamics and an Introduction to Thermostatistics* (J. Wiley & Sons, New York, 1985).

[2] *Reflections on the Motive Power of Heat and on Machines Fitted to Develop That Power*, edited by S. Carnot and R. H. Thurston (J. Wiley & Sons, New York, 1890).

[3] Y. B. Band, O. Kafri, and P. Salamon, Finite time thermodynamics: Optimal expansion of a heated working fluid, J. Appl. Phys. **53**, 8 (1982).

[4] D. A. Sivak and G. E. Crooks, Thermodynamic Metrics and Optimal Paths, Phys. Rev. Lett. **108**, 190602 (2012).

[5] P. R. Zulkowski and M. R. DeWeese, Optimal control of over-damped systems, Phys. Rev. E **92**, 032117 (2015).

[6] U. Seifert, Stochastic thermodynamics, fluctuation theorems and molecular machines, Rep. Prog. Phys. **75**, 126001 (2012).

[7] C. Jarzynski, Equalities and inequalities: Irreversibility and the second law of thermodynamics at the nanoscale, Annu. Rev. Condens. Matter Phys. **2**, 329 (2011).

[8] *Nonequilibrium Statistical Physics of Small Systems*, edited by R. Klages, W. Just, and C. Jarzynski (Wiley-VCH Verlag, Weinheim, 2013).

[9] C. Van den Broeck and M. Esposito, Ensemble and trajectory thermodynamics: A brief introduction, Physica A **418**, 6 (2015).

[10] D. J. Evans, E. G. D. Cohen, and G. P. Morriss, Probability of Second Law Violations in Shearing Steady States, Phys. Rev. Lett. **71**, 2401 (1993).

[11] D. J. Evans and D. J. Searless, Equilibrium microstates which generate second law violating steady states, Phys. Rev. E **50**, 1645 (1994).

[12] G. Gallavotti and E. G. D. Cohen, Dynamical Ensembles in Nonequilibrium Statistical Mechanics, Phys. Rev. Lett. **74**, 2694 (1995).

[13] U. Seifert, Entropy Production along a Stochastic Trajectory and an Integral Fluctuation Theorem, Phys. Rev. Lett. **95**, 040602 (2005).

[14] C. Jarzynski, Nonequilibrium Equality for Free Energy Differences, Phys. Rev. Lett. **78**, 2690 (1997).

[15] G. E. Crooks, Entropy production fluctuation theorem and the nonequilibrium work relation for free energy differences, Phys. Rev. E **60**, 2721 (1999).

[16] A. C. Barato and U. Seifert, Thermodynamic Uncertainty Relation for Biomolecular Processes, Phys. Rev. Lett. **114**, 158101 (2015).

[17] T. R. Gingrich, J. M. Horowitz, N. Perunov, and J. L. England, Dissipation Bounds all Steady-State Current Fluctuations, Phys. Rev. Lett. **116**, 120601 (2016).

[18] J. M. Horowitz and T. R. Gingrich, Thermodynamic uncertainty relations constrain non-equilibrium fluctuations, Nat. Phys. **16**, 15 (2020).

[19] U. Seifert, From stochastic thermodynamics to thermodynamic inference, Annu. Rev. Condens. Matter Phys. **10**, 171 (2019).

[20] J. M. R. Parrondo, J. M. Horowitz, and T. Sagaea, Thermodynamics of information, Nat. Phys. **11**, 131 (2015).

[21] D. M. Carberry, M. A. B. Baker, G. M. Wang, E. M. Sevick, and D. J. Evans, An optical trap experiment to demonstrate fluctuation theorems in viscoelastic media, J. Opt. A: Pure Appl. Opt. **9**, S204 (2007).

[22] S. Toyabe, T. Sagawa, M. Ueda, M. Muneyuki, and M. Sano, Experimental demonstration of information-to-energy conversion and validation of the generalized Jarzynski equality, Nat. Phys. **6**, 988 (2010).

[23] V. Blickle and C. Bechinger, Realization of a micrometer-sized stochastic heat engine, Nat. Phys. **8**, 143 (2012).

[24] J. Mehl, V. Blickle, U. Seifert, and C. Bechinger, Experimental accessibility of generalized fluctuation-dissipation relations for nonequilibrium steady states, Phys. Rev. E **82**, 032401 (2010).

[25] T. Admon, S. Rahav, and Y. Roichman, Experimental Realization of an Information Machine with Tunable Temporal Correlations, Phys. Rev. Lett. **121**, 180601 (2018).

[26] D. Collin Jr, F. Ritort, C. Jarzynski, S. B. Smith, I. Tinoco, and C. Bustamante, Verification of the Crooks fluctuation theorem and recovery of RNA folding free energies, Nature (London) **437**, 231 (2005).

[27] A. Alemany, A. Mossa, I. Junier, and F. Ritort, Experimental free-energy measurements of kinetic molecular states using fluctuation theorems, Nat. Phys. **8**, 688 (2012).

[28] O.-P. Saira, Y. Yoon, T. Tanttu, M. Möttönen, D. V. Averin, and J. P. Pekola, Test of the Jarzynski and Crooks Fluctuation Relations in an Electronic System, Phys. Rev. Lett. **109**, 180601 (2012).

[29] J. V. Koski, V. F. Maisi, J. P. Pekola, and D. V. Averin, Experimental realization of a Szilard engine with a single electron, Proc. Natl. Acad. Sci. USA **111**, 13786 (2014).

[30] K. Hayashi, H. Ueno, R. Iino, and H. Noji, Fluctuation Theorem Applied to F1-ATPase, Phys. Rev. Lett. **104**, 218103 (2010).

[31] K. Hayashi, Application of the fluctuation theorem to motor proteins: From F1-ATPase to axonal cargo transport by kinesin and dynein, Biophys Rev. **10**, 1311 (2018).

[32] S. Ciliberto, Experiments in Stochastic Thermodynamics: Short History and Perspectives, Phys. Rev. X **7**, 021051 (2017).

[33] T. Schmiedl and U. Seifert, Optimal Finite-Time Process in Stochastic Thermodynamics, Phys. Rev. Lett. **98**, 108301 (2007).

[34] D. Liberzon, *Calculus of Variations and Optimal Control Theory* (Princeton University Press, Princeton, NJ, 2012).

[35] H. Then and A. Engel, Computing the optimal protocol for finite-time processes in stochastic thermodynamics, Phys. Rev. E **77**, 041105 (2008).

[36] M. Esposito, R. Kawai, K. Lindenberg, and C. Van den Broeck, Finite-time thermodynamics for a single-level quantum dot, Europhys. Lett. **89**, 20003 (2010).

[37] E. Aurell, C. Mejia-Monasterio, and P. Muratore-Ginanneschi, Optimal Protocols and Optimal Transport in Stochastic Thermodynamics, Phys. Rev. Lett. **106**, 250601 (2011); Boundary layers in stochastic thermodynamics, Phys. Rev. E **85**, 020103(R) (2012).

[38] P. Muratore-Ginanneschi, C. Mejia-Monasterio, and L. Peliti, Heat release by controlled continuous-time Markov jump processes, J. Stat. Phys. **150**, 181 (2013).

[39] S. J. Large and D. A. Sivak, Optimal discrete control: minimizing dissipation in discretely driven nonequilibrium systems, J. Stat. Mech. (2019) 083212.

[40] A. Prados, Optimizing the relaxation route with optimal control, Phys. Rev. Research **3**, 023128 (2021).

[41] M. Bauer, K. Brandner, and U. Seifert, Optimal performance of periodically driven, stochastic heat engines under limited control, Phys. Rev. E **93**, 042112 (2016).

[42] K. Takahashi, K. Fujii, Y. Hino, and H. Hayakawa, Nonadiabatic Control of Geometric Pumping, Phys. Rev. Lett. **124**, 150602 (2020).

[43] K. Funo, N. Lambert, F. Nori, and C. Flindt, Shortcuts to Adiabatic Pumping in Classical Stochastic Systems, Phys. Rev. Lett. **124**, 150603 (2020).

[44] B. Remlein and U. Seifert, Optimality of nonconservative driving for finite-time processes with discrete states, Phys. Rev. E **103**, L050105 (2021).

[45] D. A. Leigh, J. K. Y. Wong, F. Dehez, and F. Zerbetto, Unidirectional rotation in a mechanically interlocked molecular rotor, Nature (London) **424**, 174 (2003).

[46] W. R. Browne and B. L. Feringa, Making molecular machines work, Nat. Nanotechnol. **1**, 25 (2006).

[47] S. Erbas-Cakmak, D. A. Leigh, C. T. McTernan, and A. L. Nussbaumer, Artificial molecular machines, Chem. Rev. **115**, 10081 (2015).

[48] C. Pezzato, C. Cheng, J. Fraser Stoddart, and R. Dean Astumian, Mastering the non-equilibrium assembly and operation of molecular machines, Chem. Soc. Rev. **46**, 5491 (2017).

[49] O. Raz, Y. Subaşi, and C. Jarzynski, Mimicking Nonequilibrium Steady States with Time-Periodic Driving, Phys. Rev. X **6**, 021022 (2016).

[50] F. Knoch and T. Speck, Non-equilibrium Markov state modeling of periodically driven biomolecules, J. Chem. Phys. **150**, 054103 (2019).

[51] R. Dean Astumian, Adiabatic Pumping Mechanism for Ion Motive ATPases, Phys. Rev. Lett. **91**, 118102 (2003).

[52] N. A. Sinitsyn and I. Nemenman, Universal Geometric Theory of Mesoscopic Stochastic Pumps and Reversible Ratchets, Phys. Rev. Lett. **99**, 220408 (2007).

[53] J. Ohkubo, The stochastic pump current and the non-adiabatic geometrical phase, J. Stat. Mech. (2008) P02011.

[54] O. Raz, Y. Subaşi, and R. Pugatch, Geometric Heat Engines Featuring Power that Grows with Efficiency, Phys. Rev. Lett. **116**, 160601 (2016).

[55] S. Rahav, J. Horowitz, and C. Jarzynski, Directed Flow in Nonadiabatic Stochastic Pumps, Phys. Rev. Lett. **101**, 140602 (2008).

[56] V. Y. Chernyak and N. A. Sinitsyn, Pumping Restriction Theorem for Stochastic Networks, Phys. Rev. Lett. **101**, 160601 (2008).

[57] J. M. Horowitz and C. Jarzynski, Exact formula for currents in strongly pumped diffusive systems, J. Stat. Phys. **136**, 917 (2009).

[58] C. Maes, K. Netočný, and S. R. Thomas, General no-go condition for stochastic pumping, J. Chem. Phys. **132**, 234116 (2010).

[59] D. Mandal and C. Jarzynski, A proof by graphical construction of the no-pumping theorem of stochastic pumps, J. Stat. Mech. (2011) P10006.

[60] J. Ren, V. Y. Chernyak, and N. A. Sinitsyn, Duality and fluctuation relations for statistics of currents on cyclic graphs, J. Stat. Mech. (2011) P05011.

[61] S. Asban and S. Rahav, No-Pumping Theorem for Many Particle Stochastic Pumps, Phys. Rev. Lett. **112**, 050601 (2014).

[62] S. Asban and S. Rahav, Stochastic pumping of particles with zero-range interactions, New J. Phys. **17**, 055015 (2015).

[63] J. M. R. Parrondo, Reversible ratchets as Brownian particles in an adiabatically changing periodic potential, Phys. Rev. E **57**, 7297 (1998).

[64] I. M. Sokolov, A perturbation approach to transport in discrete ratchet systems, J. Phys. A: Math. Gen. **32**, 2541 (1999).

[65] S. Rahav, Extracting work from stochastic pumps, J. Stat. Mech. (2011) P09020.

[66] V. Y. Chernyak, J. R. Klein, and N. A. Sinitsyn, Quantization and fractional quantization of currents in periodically driven stochastic systems. I. Average currents, J. Chem. Phys. **136**, 154107 (2012).

[67] R. Chatterjee, S. Chatterjee, P. Pradhan, and S. S. Manna, Interacting particles in a periodically moving potential: Traveling wave and transport, Phys. Rev. E **89**, 022138 (2014).

[68] K. Brandner, K. Saito, and U. Seifert, Thermodynamics of Micro- and Nano-Systems Driven by Periodic Temperature Variations, Phys. Rev. X **5**, 031019 (2015).

[69] K. Proesmans, B. Cleuren, and C. Van den Broeck, Linear stochastic thermodynamics for periodically driven systems, J. Stat. Mech. (2016) 023202.

[70] T. Koyuk, U. Seifert, and P. Pietzonka, A generalization of the thermodynamic uncertainty relation to periodically driven systems, J. Phys. A: Math. Theor. **52**, 02LT02 (2019).

[71] A. C. Barato and R. Chetrite, Current fluctuations in periodically driven systems, J. Stat. Mech. (2018) 053207.

[72] N. A. Sinitsyn, The stochastic pump effect and geometric phases in dissipative and stochastic systems, J. Phys. A: Math. Theor. **42**, 193001 (2009).

[73] R. Dean Astumian, Stochastic conformational pumping: A mechanism for free-energy transduction by molecules, Annu. Rev. Biophys. **40**, 289 (2011).

[74] R. D. Astumian, Stochastic pumping of non-equilibrium steady-states: How molecules adapt to a fluctuating environment, Chem. Commun. **54**, 427 (2018).

[75] Z. Wang, L. Wang, J. Chen, C. Wang, and J. Ren, Geometric heat pump: Controlling thermal transport with time-dependent modulations, Front. Phys. **17**, 13201 (2022).

[76] M. I. Zelikin and V. Borisov, *Theory of Chattering Control* (Birkhäuser, Boston, 1994).

[77] C. Edwards and S. K. Spurgeon, *Sliding Mode Control: Theory and Applications* (Taylor & Francis, New York, 1998).

[78] J. Howard, *Mechanics of Motor Proteins and the Cytoskeleton* (Sinauer Assoc., Sunderland, MA, 2001).

[79] P. Hänggi, P. Talkner, and M. Borkovec, Reaction-rate theory: Fifty years after Kramers, Rev. Mod. Phys. **62**, 251 (1990).

[80] M. R. Wilson, J. Sola, A. Carlone, S. M. Goldup, N. Lebrasseur, and D. A. Leigh, An autonomous chemically fuelled small-molecule motor, Nature (London) **534**, 235 (2016).

[81] T. Duriez, S. L. Brunton, and B. R. Noack, *Machine Learning Control—Taming Nonlinear Dynamics and Turbulence* (Springer, Switzerland, 2017).

[82] A. Gal and O. Raz, Precooling Strategy allows Exponentially Faster Heating, Phys. Rev. Lett. **124**, 060602 (2020).